A DUAL-SCALE APPROACH FOR REPRESENTING SOLIDIFICATION IN THE INTEGRATED FLOW-STRESS MODEL FOR PREPREG PROCESSING

Fahimi, Shayan[1]*, Forghani, Alireza[2], Vaziri, Reza[1], Poursartip, Anoush[1,2]
[1] Composites Research Network (CRN), Departments of Civil Engineering and Materials Engineering, The University of British Columbia, Vancouver, Canada
[2] Convergent Manufacturing Technologies Inc, Vancouver, Canada
* Corresponding author (shayan@composites.ubc.ca)

Keywords*: Composite processing, Integrated flow-stress model, Finite Element Analysis*

1 ABSTRACT

Science-based simulation methods can significantly mitigate the uncertainty risk involved in modifying established composites manufacturing processes. For prepreg processing, the first generation of flow-stress models presented a sequential coupling between the flow model, based on Darcy's flow, and Terzaghi's effective stress model to predict the resin content and residual stresses at the end of a cure cycle. The sequential coupling is not able to capture the more complex two-way interactions between deformation and resin flow. To integrate the governing equations of flow and stress modules, a state variable called solidification factor (λ), has been introduced in the second generation of flow-stress models (a.k.a. integrated flow-stress or IFS model). This state variable indirectly controls the pressure sharing between the fluid and solid phase and the effective shear and bulk moduli of the composite system. However, in the current IFS model, the solidification factor has been defined as an arbitrary function of the degree of cure rather than in terms of measurable mechanical properties of the constituents. Moreover, it has been assumed that the shear and bulk moduli of the composite change linearly with the solidification factor.

In this study, to build a model capable of simulating intermediate cool-downs in which the temperature is reduced with an increasing or constant degree of cure, λ is defined as a function of both the degree of cure (χ) and temperature (T). The solidification factor calculated from experimental data is used as boundary conditions to determine the contours of solidification factors over the process map. By taking into account the spatial distribution of λ over a hexagonal representative volume element of fibre and matrix, the effective shear and bulk moduli of prepreg are calculated and compared with the literature. Since the solidification factor is a history-dependent variable, this work also proposes further experiments to characterize λ.

2 INTRODUCTION

The distinguishing characteristic of composite manufacturing is that the material and the final part are engineered simultaneously [1]. Extensive changes in physical and chemical properties, as well as significant changes that occur in constituents' bulk and shear moduli, make the process modelling of composite materials extremely challenging. It is well-established that the processing operation will result in a two-scale flow and that there are four processes occurring simultaneously: deformation of individual plies (meso-scale), deformation of the entire preform

(macro-scale), infiltration of resin into individual tows (micro-scale), and infiltration of resin into the channels (macro-scale).

For prepreg processing, the first generation of flow-stress models presented a sequential coupling between the flow model, based on Darcy's flow [2], and Terzaghi's effective stress model [3] to predict the resin content and residual stresses at the end of a cure cycle. The sequential coupling is not able to capture the more complex two-way interactions between deformation and resin flow. To integrate the governing equations of flow and stress modules, a state variable called solidification factor (λ), has been introduced in the second generation of flow-stress models (a.k.a. integrated flow-stress or IFS model) [4], [5]. This state variable indirectly controls the pressure sharing between the fluid and solid phase and the effective shear and bulk moduli of the composite system. In the original IFS model, the solidification factor has been defined as an arbitrary function of the degree of cure rather than in terms of measurable mechanical properties of the constituents. Moreover, it has been assumed that the shear and bulk moduli of the composite vary linearly with the solidification factor.

In this study, λ is defined as a function of measurable state variables of the system, the degree of cure and temperature, and its path dependency is explored. The solidification factor calculated from experimental data is used as boundary conditions to determine contours of the solidification factor over the process map. By taking into account spatial distribution of λ over a hexagonal representative volume element (RVE) of fibre and matrix, the effective shear and bulk moduli of prepreg are calculated and compared with corresponding values reported in the literature. Since the solidification factor is a history-dependent variable, this work also proposes further experiments to characterize λ.

3 PROBLEM FORMULATION (U-P FORM)

The original integrated flow-stress model was formulated in the u-v-p form, where solid displacement, *u*, fluid velocity, *v,* and pressure, *p,* constitute the element nodal degrees of freedom. To implement the model in commercial finite element software, such as ABAQUS, it is reformulated in the u-p form, where the velocity is determined in a post-processing step using the Darcy's equation. The mass conservation equation for both the original and u-p formulation is shown in Table 1:

Table 1: Comparison between the u-p and the original form of the mass conservation equation for the integrated flow-stress model

Original formulation	Current (u-p) formulation
Mass conservation: $\boldsymbol{\beta \frac{D}{Dt} u^S_{i,i} - v^F{}_{i,i} + \left(\frac{\beta - \varphi^F}{K^S} + \frac{\varphi^F}{K^F}\right)\frac{D\ p}{Dt} - (1-\varphi^F)(1-\lambda)\frac{D}{Dt}e^S_0}$ $\boldsymbol{- \varphi^F(1-\lambda)\frac{D}{Dt}e^F_0 - \frac{1}{3K^S}D^{SK}\frac{D}{Dt}e^{SK}_0 = 0}$ **Darcy's flow**: $\boldsymbol{p^F_{,i} + \mu^F S^{-1} v^F{}_i = 0}$	**Mass conservation:** $\beta \frac{D}{Dt} u^S_{i,i} - \frac{S}{\mu} p_{,ii} + \left(\frac{\beta - \varphi^F}{K^S} + \frac{\varphi^F}{K^F}\right)\frac{D\ p}{Dt} - (\beta - \varphi^F)\frac{D}{Dt}e^S_0$ $- \varphi^F \frac{D}{Dt} e^F_0 = 0$

where $\frac{D}{Dt}$ denotes material derivative, u , p, and v are the deformation, pressure, and velocity (all unknowns), respectively. S is the permeability tensor, K is the bulk modulus and D is the fourth-order elastic tensor. ρ is the density, φ is the volume fraction, β is the Biot's coefficient, μ is the viscosity, and superscripts S, SK, and F

represent the solid (fibre), solid-skeleton (fibre-bed and solidified resin), and fluid phases, respectively. Also, e_0 is the free strain, due to thermal expansion and cure shrinkage.

During the solidification process, the resin properties become a mixture of those in the fluid and solid state of the resin. If the viscosity remains low, the evolution of resin material properties should not change our fundamental assumption for using flow through porous media, however, a jump in resin viscosity over a certain threshold would hinder all resin movements and thus make the porous media assumption inapplicable. Experimental observations show that the following properties change during the solidification process:

1. Permeability of the fibre-bed for resin and gas flow [6]
2. Resin cure shrinkage coefficient and thermal expansion coefficient [7]
3. Bulk and shear modulus of the resin ([7])
4. Bulk and shear modulus of the fibre-bed [2]

Amini [4] incorporated the above-mentioned effects by introducing a new scalar quantity, λ, termed 'solidification factor', which is bounded between zero and one ($\lambda = 0$ for unsolidified resin and $\lambda = 1$ for fully solidified resin). The stiffness of the solid and solid skeleton are defined as functions of the solidification factor (Equation 1). With this assumption, as the resin cures, the solid skeleton transforms from a porous medium consisting of individual fibres into a combination of fibres and load (shear)-bearing resin.

$$K^{SK} = \lambda\left(K^{c} - K^{fb}\right) + K^{fb} \tag{1}$$

where K^{c} and K^{fb} are the bulk modulus of the solid composite, obtained from micromechanical models, and the bulk modulus of the fibre-bed, obtained from the Gutowski model [8]. The bulk modulus of the solid-skeleton is an input of the integrated flow-stress model.

The mass conservation should be coupled with the momentum conservation equation, Equation 2, to solve for the unknown pressure and deformation.

$$\frac{D}{Dt}\sigma_{ij} = D^{SK}\left(\frac{D}{Dt}\varepsilon_{ij}^{S} - \frac{D}{Dt}{\varepsilon_{ij}}_{0}^{S}\right) - \frac{D}{Dt}(\beta p^{F})I_{ij} \tag{2}$$

where $\frac{D}{Dt}\sigma_{ij}$ and $\frac{D}{Dt}\varepsilon_{ij}^{S}$ represent the rate of total stress and strain, respectively. A pseudo-viscoelastic, viscoelastic, or thermo-viscoelastic constitutive model might be used with the governing equations to describe the behaviour of the solid skeleton. The finite element implementation is achieved by deriving the weak form of the governing differential equations using the Galerkin method. The discretized form of the governing and the constitutive equations are implemented in ABAQUS using UserElement (UEL) and UserMaterial (UMAT) modules, respectively.

4 SOLIDIFICATION AS A FUNCTION OF CURE AND TEMPERATURE

The integrated flow-stress (IFS) formulation uses the solidification factor to keep a single set of equations applicable to the whole manufacturing process. While the solidification factor is only a function of the degree of cure, it is not possible to add the effects of temperature, melting at high temperatures and solidifying at low temperatures. To further illustrate this point, a process map is shown in Figure 1-a. All processes in a process map are constructed of a combination of the following four types of processes:

A. Curing and isothermal ($\Delta T = 0$)
B. Curing and heat-up ($\Delta T > 0$)
C. Curing and cool-down ($\Delta T < 0$)

D. No curing and cool-down ($\Delta T < 0$)

The original flow-stress model with a solidification factor that is only a function of the degree of cure provides the necessary functionalities to simulate processes A and B. In general, relating the solidification factor only to the degree of cure works when temperature and degree of cure are changing in the same direction. However, in processes C and D, the temperature is decreasing while the degree of cure is constant or increasing.

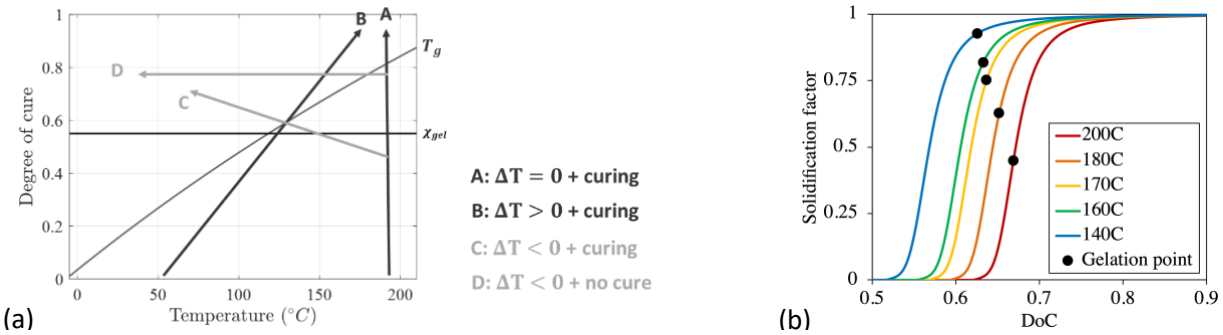

Figure 1: (a) A composite process map with four main types of processes, and (b) the solidification curve for curing with different hold temperatures, replicated with permission from Reference [9]

Recent work by Naito [9] presented some candidate functions to determine the solidification factor based on measurement of shear moduli during the curing process. One such function is shown in Equation 3:

$$\lambda = \frac{\partial(\log_{10} G^{SK})/\partial(\log_{10} G^{r})}{\partial(\log_{10} G^{SK})/(\log_{10} G^{r})} \quad (3)$$

where *G* stands for shear modulus and the superscript *r* refers to resin. Figure 1-b shows the solidification curve predicted by Equation 3 for curing a select resin system undergoing a series of one-hold cure cycles with varying hold temperatures and constant heating rate of $4°C$ /min. The gelation point is defined to be the instant when the storage and loss moduli for the resin system in the rheometer test coincide, i.e. $G' = G''$. These experiments show that lower hold temperatures in one-hold cure cycles result in early solidification. Moreover, it is evident that the gelation point in cycles with different hold temperatures occurs at different temperatures and degrees of cure (DoC), showing the path dependency of the solidification factor.

To simulate process D, the solidification factor should be characterized as a function of temperature and degree of cure at any point on the process map. In the original IFS model, the current state of cure was compared with the degree of cure at gelation to determine the solidification factor. Given that solidification is a function of both temperature and degree of cure, we propose to calculate the solidification factor by finding the minimum distance between the current state of the system, identified by the pair of temperature and degree of cure, and the T_g curve on the process map.

While the solidification factor is a path-dependent variable, sufficient experimental data is not available to investigate its path dependency by linking it to the rate of the degree of cure or temperature. Instead, a set of solidification contours, one for each hold temperature, are calculated using the data obtained from the corresponding experiment as boundary conditions. Triple values of the degree of cure at 1% solidification, the degree of cure and solidification at gelation point, and the degree of cure at 99% solidification are chosen to bound the values of solidifaction factor between $\lambda = 0$ and $\lambda = 1$. These contours are shown in Figure 2.

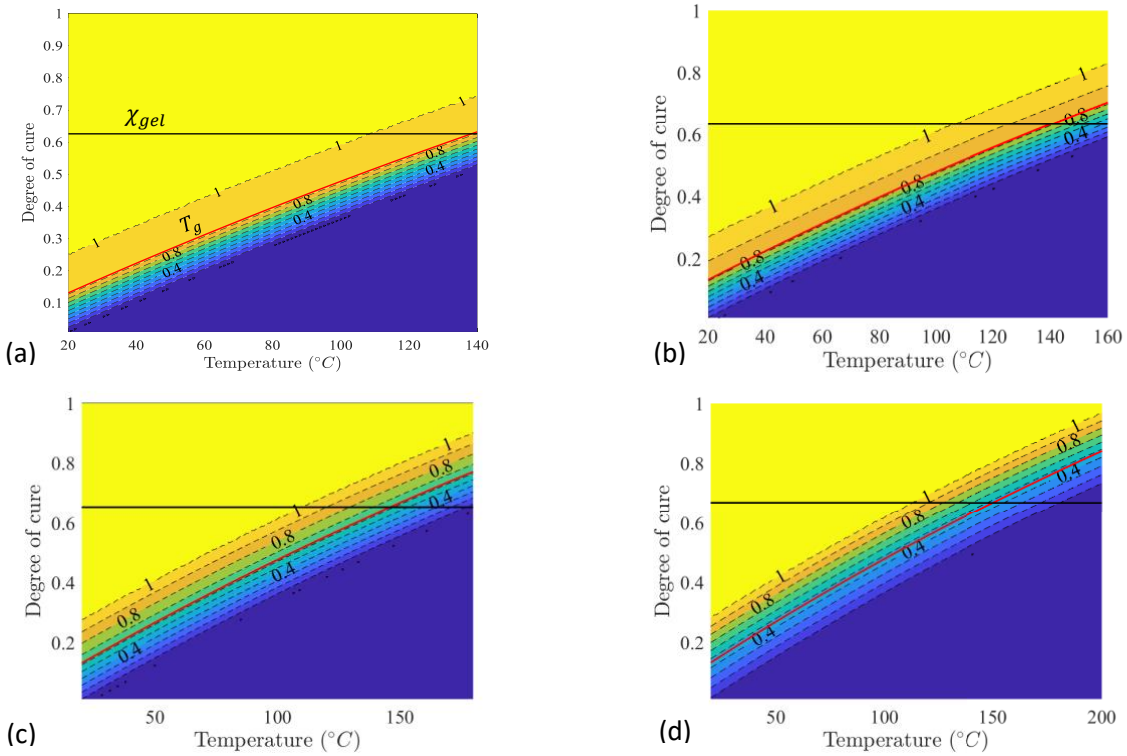

Figure 2: Contours of solidification factor λ as a function of degree of cure and temperature $\lambda = f(\chi, T)$ at (a) T_{hold} = 140°C, (b) T_{hold} = 160°C, (c) T_{hold}= 180°C, and (d) T_{hold}= 200°C

The model described in this section can be used to estimate the solidification factor at any point in the process map and is not confined to the points recorded during the experiments.

5 MULTISCALE SOLIDIFICATION

A built-in assumption in Niaki's model [4] is that the properties of the composite vary linearly with solidification. Also, it is assumed that the material properties of the composite at any stage during the cure can be calculated using analytical micromechanics [4].

The nonuniformity of the degree of cure and temperature at the microscale leads to different solidification and flow behaviour inside an RVE. Thus, an accurate representation of the RVE should incorporate the spatial variation of solidification and cure. Malekmohammadi [10] developed a microscale model for evaluating the bulk and shear moduli of composites with different fibre-to-resin ratios. In this work, we use the same procedure with the 2D flow model to determine the properties of the composite during the curing process.

Hashin and Rosen [11] proposed the Composite Cylinders Assemblage (CCA) model (Figure 3-a) to estimate the effective properties of unidirectional cylindrical fibre composites. They obtained closed-form expressions for four effective elastic moduli and found bounds for the fifth elastic modulus of transversely isotropic fibre composites.

Since the analytical micromechanics equations are derived for fully-solid composites, new methods should be used to properly incorporate the effect of liquid resin in these micromechanics models. Numerical approaches are promising for estimating the effective properties of composites in these scenarios. Another reason for using numerical methods is the nonuniformity of degree of cure and temperature at the microscale that causes different solidification and flow behaviour inside an RVE. Since the thermal conductivity of carbon fibre, especially along the fibre direction, is higher than that of resin, we can reasonably assume that the temperature and degree of cure are higher around the fibres. In other words, at the microscale level, the resin builds entanglements around fibres first and then the chains are extended into areas far from the surface of the fibres. The normal distance between the fibre surface and a point in the resin can be used to build a degree of cure and solidification factor distribution inside the RVE. Figure 3-b shows the contour of the normal distance between the center of elements in the region filled with resin with the nearest fibre surface, Δ, in the hexagonal RVE.

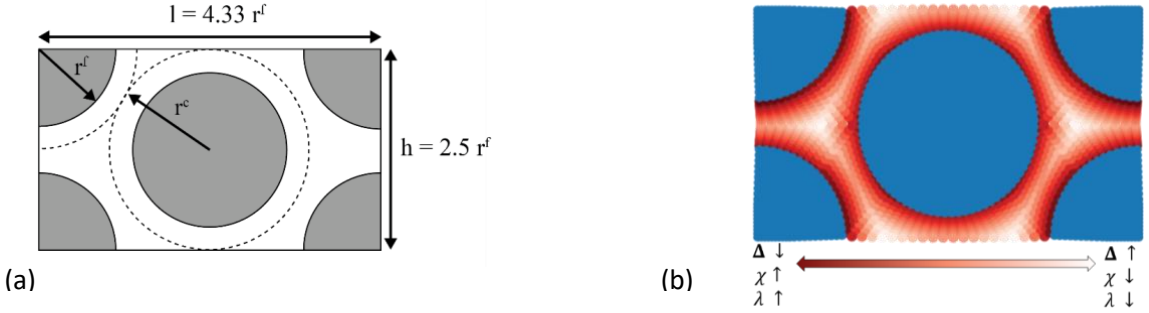

Figure 3: (a) Geometry of the hexagonal unit cell with fibre volume fraction, $\varphi^f = 0.58$, and (b) distribution of Δ in the hexagonal RVE

By matching the distance of each element center from the nearest fibre surface, Δ, with the element surface area, a distribution for Δ can be found and consequently, a contour of degrees of cure and solidification factors can be determined that averages out to the macroscale properties. The distribution of the degree of cure in the RVE is obtained by setting the area-weighted degree of cure equal to the macroscopic degree of cure and assuming an arbitrary maximum deviation from the average, such as ± 0.05 cure. As an example, if the average degree of cure is 0.2, the range of degree of cure in the RVE is $[0.1681, 0.25]$.

To evaluate this model, the elastic properties predicted by the numerical finite element model are compared with analytical models and previous numerical results. The numerical approach is used to predict the elastic properties of AS4/3501-6 composites with fibre volume fraction, $\varphi^f = 0.58$.

The results of the current multiscale model are compared with the "Original 2PIFS" model in Table 3. The "Original 2PIFS" results show the elastic properties calculated using the model developed by Niaki [4]. The model determines the solidifying composite properties by averaging the fibre-bed and fully-solidified composite properties using the solidification factor as the averaging weight. The original 2PIFS model and the multiscale model predict the same properties for fully-solidified composite since the distribution of degree of cure and solidification does not appear in this case. Compared to the original 2PIFS model, the multiscale model predicts stiffer elastic moduli when the material is solidifying. The discrepancy between the two models is around 11% for E_1 and 35% for E_2.

While performing microscale RVE calculations is not feasible at every time step, a look-up table can be generated by finding the material properties of the RVE for different solidification factors and fibre volume fractions prior to the analysis. Such a table is used in the next section to find the properties of the system at each time step. After finding the solidification factor from temperature and degree of cure, the look-up table constructed using the microscale model can be used to find the mechanical properties of the prepreg.

Table 2: Engineering constants for AS4/3501-6 composite with $\varphi^f = 0.58$ at various values of solidification factor

	Numerical ($\lambda = 1.0$)		Numerical ($\lambda = 0.5$)		Numerical ($\lambda = 0.1$)	
Property	**Original IFS**	**Multiscale model**	**Original IFS**	**Multiscale model**	**Original IFS**	**Multiscale model**
E_1 (GPa)	115.15	115.15	110.71	114.42	102.14	113.83
E_2 (GPa)	7.81	7.81	4.00	4.59	0.80	1.08
G_{12} (GPa)	3.61	3.61	1.94	1.92	0.39	0.40
G_{23} (GPa)	2.61	2.61	1.39	1.55	0.28	0.37
ν_{12} (GPa)	0.26	0.26	0.24	0.26	0.21	0.26
ν_{23} (GPa)	0.44	0.44	0.37	0.44	0.31	0.45

6 BENDING MOMENT AND SHEAR FORCE OF ANGLE LAMINATE

As an example, an L-shaped unidirectional [0°] laminate, shown in Figure 4-a is considered that undergoes the two-hold cure cycle (Figure 4-b). The top surface is under a 540 kPa pressure and the top and side surfaces are permeable and the initial volume fraction of fibres is $\varphi_0^f = 0.58$. While the characterized material model for AS4-3501-6 is not perfect, in order to compare the outcome of the current model with previously published research, AS4-3501-6 material system is used in this section.

A finite element model of the angle laminate is built in ABAQUS and the solidification factor and material properties characterized using the methods described in the previous section are used to determine the response of the composite part during the cure cycle. Different element sizes are used for mesh convergence studies and a 72 by 12 discretization is chosen to report the results.

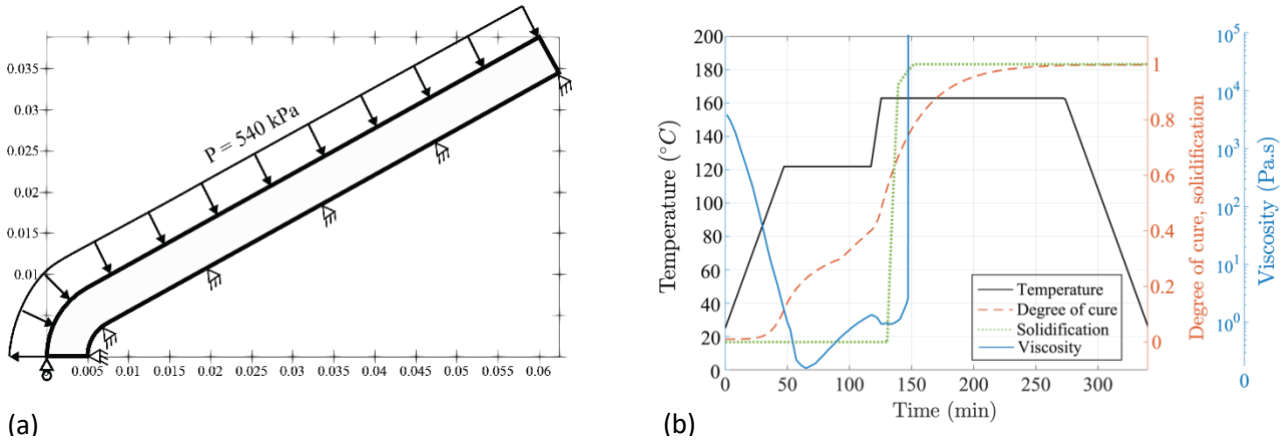

(a) (b)

Figure 4: a) the geometry of the angle laminate and b) temperature, degree of cure, viscosity, and solidification factor in the angle-laminate cure cycle

Figure 5 shows the distribution of the resultant axial force and bending moment along the mid-plane of the angle laminate at three instants of time, before solidification ($t = 137$ min), after the second hold ($t = 285$ min), and at

the end of the cure cycle ($t = 340\ min$). Comparison is made between the predictions of the sequential (first generation) flow-stress model, original IFS model, and current model with pseudo-viscoelastic and viscoelastic material models. The internal bending moment distribution of the part reflects the residual stress build-up in the final part and hence its shape after tool removal. At all instants of time, the predictions of the current model are found to be closer to the integrated flow-stress model since both models include the early effects of resin flow around the corner on the response of the final part. At $t = 137\ min$, the difference between the current and the original IFS is negligible, since the material properties used in both models are similar. Compared to the original IFS, solidification starts earlier in the current multiscale IFS and the solid skeleton is stiffer (see Table 2). Thus, at the end of the second hold, $t = 285\ min$, the multiscale IFS with pseudo-viscoelastic material model predicts higher bending moment and axial force resultants. The difference between the pseudo-viscoelastic and viscoelastic material model is more evident at the end of the cure cycle ($t = 340\ min$) when the relaxation of the residual stresses leads to lower bending moment and axial force compared to the pseudo-viscoelastic material model.

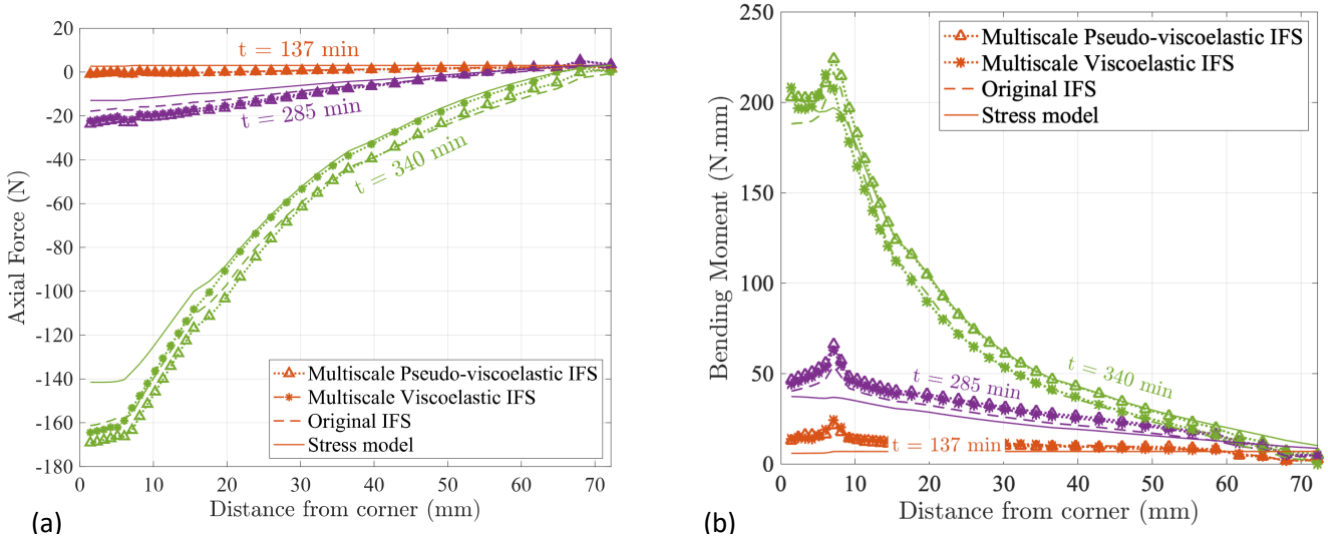

Figure 5: The distribution of the resultant a) axial force and b) bending moment along the mid-plane of the prepreg laminate at three instants of time

7 CONCLUSION

The original integrated flow-stress model used a state variable termed the solidification factor, λ, to link the conservation of mass and momentum equations and update the material properties of the composite system during the curing process. However, λ was not characterized based on measurable properties of the composite system and the material properties of the solidified composite were determined by taking the weighted average (using λ as the weighting factor) of the resin and fibre-bed properties.

Building on previous work [9], the current work presents a method to characterize the solidification factor based on the shear moduli recorded during the curing process. Since the solidification factor is a path-dependent parameter, further experiments with different heating rates up to the hold temperature are required to provide sufficient data to study the effect of heating rate ($\frac{dT}{dt}$) and rate of change of the degree of cure ($\frac{d\chi}{dt}$) on the solidification factor.

Moreover, we presented a method to compute the solid skeleton properties based on the properties of the resin and fibre by incorporating the spatial variation of the degree of cure and solidification into a numerical micromechanics model based on a hexagonal fibre packing that is consistent with the assumptions of CCA. In the pre-gelation phase, the assumptions of no-slip boundary conditions between the fibre and resin and the periodic boundary conditions typically used in numerical micromechanical models of solid phases may not be applicable. Therefore, to relax these assumptions, a discrete micromechanical model is being developed to determine the material properties of the fibre bed during the early stages of the curing process [12].

The resultant bending moment and axial force on the midplane of an angle laminate obtained from the multiscale IFS are compared with those determined from previous generations of the process model to study the effect of the new modifications to the model. With the proposed changes in the characterization of the solidification factor, the current model shows an earlier onset of solidification that results in higher residual stresses and hence higher bending moments and axial forces. Replacing a pseudo-viscoelastic material model with a viscoelastic material model has negligible effects on the bending moment and axial force before the onset of solidification, however, viscoelastic relaxation comes into play as resin solidification progresses.

8 REFERENCES

[1] J. Fabris, D. Roughley, A. Poursartip, and E. Maine, “Managing the technological and market uncertainty of composites innovation: a case study of composites manufacturers in Western Canada and interventions by a translational research centre,” *Transl. Mater. Res.*, vol. 4, no. 4, p. 046001, Nov. 2017,

[2] P. Hubert and A. Poursartip, “Aspects of the Compaction of Composite Angle Laminates: An Experimental Investigation,” *J. Compos. Mater.*, vol. 35, no. 1, pp. 2–26, Jan. 2001,

[3] A. Johnston, R. Vaziri, and A. Poursartip, “A Plane Strain Model for Process-Induced Deformation of Laminated Composite Structures,” *J. Compos. Mater.*, vol. 35, no. 16, pp. 1435–1469, Aug. 2001,

[4] S. A. Niaki, A. Forghani, R. Vaziri, and A. Poursartip, “A three-phase integrated flow-stress model for processing of composites,” *Mech. Mater.*, vol. 117, pp. 152–164, Feb. 2018,

[5] S. A. Niaki, A. Forghani, R. Vaziri, and A. Poursartip, “A two-phase integrated flow-stress process model for composites with application to highly compressible phases,” *Mech. Mater.*, vol. 109, pp. 51–66, Jun. 2017,

[6] S. S. Tavares, V. Michaud, and J.-A. E. Månson, “Through thickness air permeability of prepregs during cure,” *Compos. Part Appl. Sci. Manuf.*, vol. 40, no. 10, pp. 1587–1596, Oct. 2009,

[7] I. Baran, K. Cinar, N. Ersoy, R. Akkerman, and J. H. Hattel, “A Review on the Mechanical Modeling of Composite Manufacturing Processes,” *Arch. Comput. Methods Eng.*, vol. 24, no. 2, pp. 365–395, Apr. 2017,

[8] Z. Cai and T. Gutowski, “The 3-D Deformation Behavior of a Lubricated Fiber Bundle,” *J. Compos. Mater.*, vol. 26, no. 8, pp. 1207–1237, Aug. 1992,

[9] Y. Naito, “A study on deformation of unidirectional prepreg for thermoset-based CFRP during cure,” Ph.D. Thesis, Kyoto University, 2022.

[10] S. Malekmohammadi, “Efficient multi-scale modelling of viscoelastic composites with different microstructures,” Ph.D. Thesis, University of British Columbia, 2014.

[11] Z. Hashin and B. W. Rosen, “The Elastic Moduli of Fiber-Reinforced Materials,” *J. Appl. Mech.*, vol. 31, no. 2, pp. 223–232, Jun. 1964,